Towards Integrated design of fluidic flight controls for a flapless aircraft

W. J. Crowther
bill.crowther@manchester.ac.uk

P. I. A. Wilde, K. Gill and S. M. Michie
University of Manchester
Manchester, UK

ABSTRACT

Fluidic flight controls enable forces and moments for flight vehicle trim and manoeuvre to be produced without use of conventional moving surface controls. This paper introduces a methodology for the design of Circulation Control (CC) and Fluidic Thrust Vectoring (FTV) as fluidic controls for roll and pitch. Work was undertaken as part of the multidisciplinary FLAVIIR project, with the goal of providing full authority fluidic flight controls sufficient for a fully flapless flight of an 80kg class demonstrator aircraft known as DEMON. The design methodology considers drag, mass, volume and pneumatic power requirements as part of the overall design cost function. It is shown that the fundamental flow physics of both CC and FTV are similar, and hence there are strong similarities to the design approach of each. Flight ready CC and FTV hardware has been designed, manufactured and ground tested. The CC system was successfully wind tunnel demonstrated on an 85% scale half model of the DEMON. The design condition of a control ΔC_L of 0·1 was achieved with a blowing coefficient of 0·01, giving a useable control gain of 10. The FTV system was static tested using a micro gas turbine source. The control characteristic was '*N*' shaped, consisting of an initial high gain response in a negative sense (gain = –30) followed by a low gain response in a positive sense (gain = +3) at higher blowing rate. CC and FTV control hardware directly contributes to around 6% to the overall mass of the flight vehicle, however provision of pneumatic power carries a significant mass penalty unless generated as part of an integrated engine bleed system.

NOMENCLATURE

a	gain
A	area (m^2)
AR	aspect ratio
b	spanwise width of manoeuvre effector (m)
c	mean aerodynamic chord (m)
C_D	drag coefficient
C_h	slot curvature h/R
C_L	lift coefficient
C_M	pitching moment coefficient
C_μ	blowing coefficient
CR	contraction ratio H/h
C_R	rolling moment coefficient
C_y	y force coefficient
C_z	z force coefficient
d	chordwise length of manoeuvre effector (m)
F_z	z force
h	slot height (m)
H	plenum height at the inlet (m)
M	Mach number
p	roll rate (rad/s), pressure (Pa)
$\dot{p}$	roll acceleration (rad/s^2)
q	dynamic pressure (kg/ms^2)
R	Coanda surface radius (m)
s	semispan (m)
U	velocity (ms^{-1})
xyz	body axis system
δ	boundary-layer thickness (m)

Paper No. 3406. Manuscript received 12 February 2009, revised version received 10 July 2009 accepted 6 August 2009.

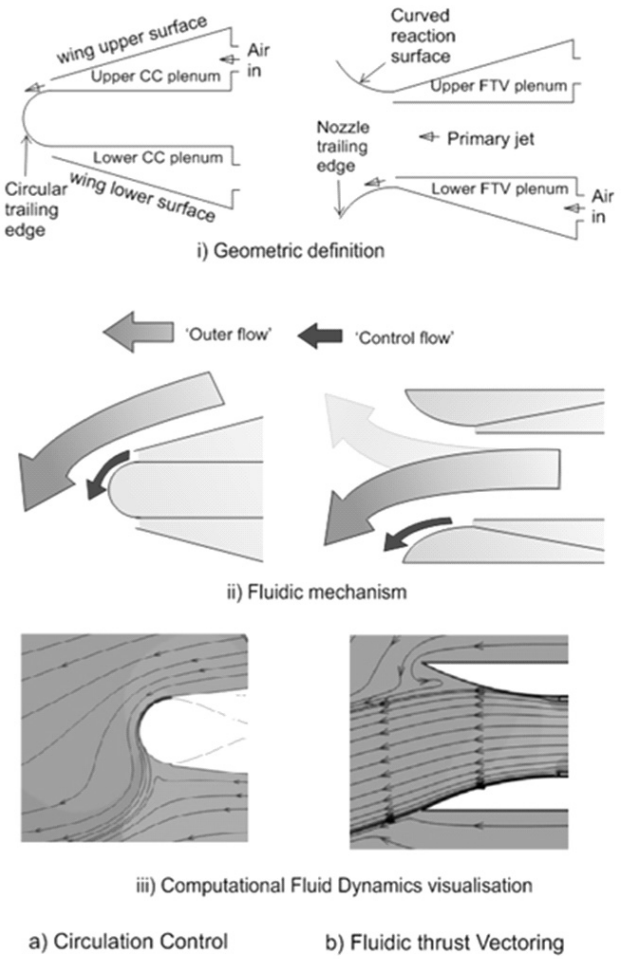

Figure 1. Introduction to the concepts of Circulation Control and Fluidic Thrust Vectoring.

η efficiency
ρ density (kg/m^3)
θ_T Coanda surface termination angle (deg)
$\dot{\theta}$ pitch rate (rad/s)

Subscripts

i inlet
j jet
o outlet
p primary or plenum
s secondary
0 total conditions
∞ free stream

Abbreviations

APU auxiliary power unit
CC circulation control
FTV fluidic thrust vectoring
PPS pneumatic power supply

1.0 INTRODUCTION

Integration of Fluidic Thrust Vectoring (FTV) and Circulation Control (CC) onto an airframe provides the capability to trim and manoeuvre without use of conventional control surfaces. The three main design requirements for flapless controls are that:

1. they should be effective, i.e. produce forces and moments of sufficient magnitude to control the aircraft over the desired flight envelope;
2. they should be efficient, i.e. produce the required forces and moments using the minimum amount of power, and
3. the overall systems cost of implementing the controls should be consistent with the benefits that the flapless controls bring to the overall aircraft system.

https://doi.org/10.1017/S0001924000003365 Published online by Cambridge University Press

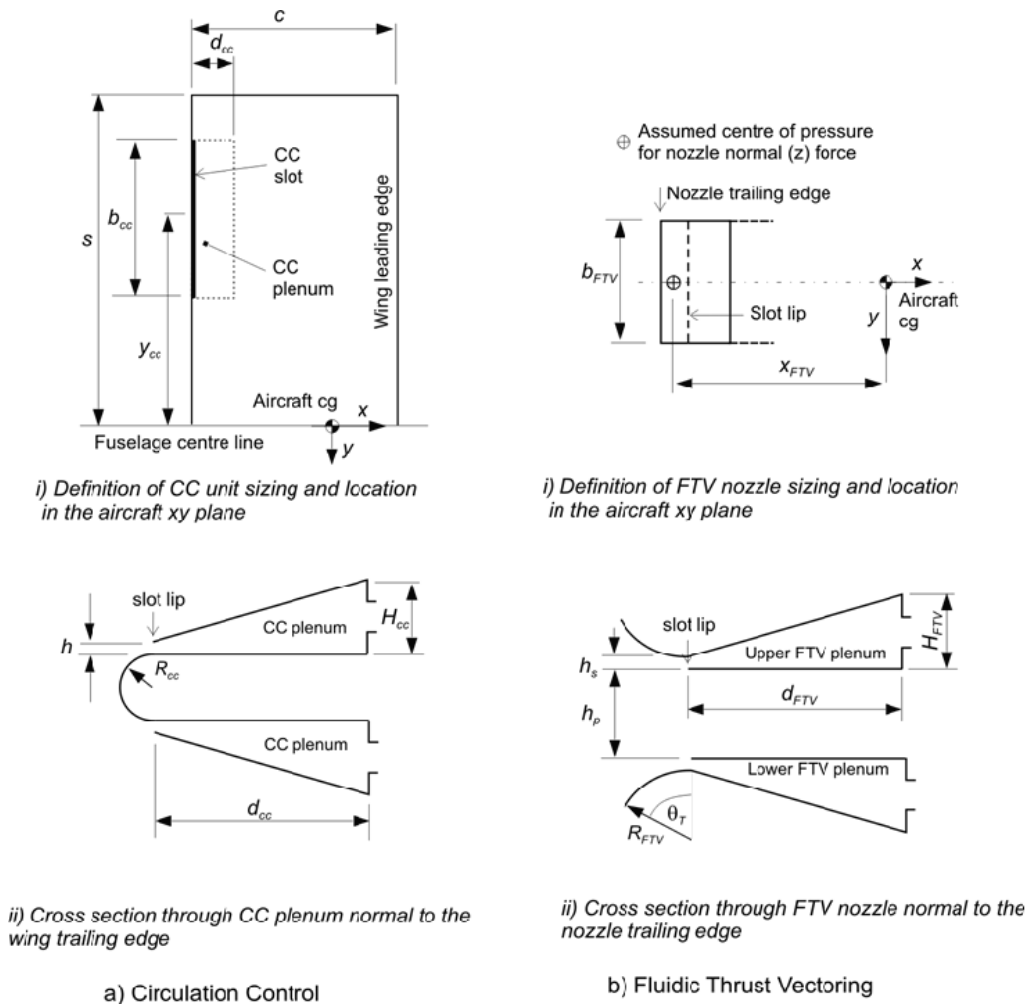

Figure 2. Geometry definition for CC and FTV hardware.

CC has been widely studied in the literature[1-7] and the concept may be thought of as well understood; however, most of this work has focussed on application of CC for high lift rather than as a flight control. With regard to thrust vectoring, there has been extensive previous research into both mechanical[8-12] and fluidic thrust vectoring[13-16] systems for control applications. However, the possible design space for FTV is more complex than for CC due to the potentially large Mach number range of interest and nozzle exit geometry constraints. In comparison with CC, no single approach has emerged as generally applicable.

The flow physics of CC and FTV are broadly similar in that they both use a rectangular curved wall jet to control an outer flow[17]. The generic geometry and fluid mechanisms associated with CC and FTV are illustrated in Fig. 1. For the CC case, the outer flow is the free stream flow around a wing, whereas for FTV, the outer flow is the propulsive exhaust flow. Both devices require a pair of secondary jets to achieve both positive and negative control forces in the plane of operation, however, for the CC the reaction surfaces are combined into a single curved trailing edge, whereas for FTV two spatially separated reaction surfaces are required. The FTV arrangement gives the possibility that the 'outer' flow can attach to either of two reaction surfaces. In practice this gives rise to two different control modes: a 'reverse' mode in which the main jet attaches to the reaction surface on the opposite side to the control jet, and a 'forward' mode where the main jet attaches to the adjacent reaction surface. This has important consequences and is discussed in some detail in the FTV experimental results section. The plenum requirements are similar in both cases, and the practicality of both controls depends on the fluid momentum amplification provided by the control geometry.

Historically, there are few examples of successful long term implementation of flow control technology on production aircraft. The main reason for lack of success would appear not to be lack of effectiveness; rather, the benefits of application have not exceeded the cost of implementation. In light of this, this paper focuses on the development of a methodology for the design of CC and FTV that provides initial consideration of integration issues associated with weight, power and drag. Understanding of critical CC/FTV-related engineering design trades can be made by addressing some of the system costs in parallel with the aerodynamic performance costs, and this will hopefully lead to more globally optimised designs for flapless aircraft.

2.0 FLUIDIC CONTROL DESIGN METHODOLOGY

2.1 Overview

The purpose of this section is to define a design methodology for preliminary sizing of CC and FTV fluidic flight controls. The design method is 'integrated' with respect to the design of the whole aircraft

https://doi.org/10.1017/S0001924000003365 Published online by Cambridge University Press

in the sense that it considers the potential drag penalty associated with the control, the plenum geometry and volume, and the Pneumatic Power Supply (PPS) mass flow and pressure requirements as part of the overall design cost function.

The geometric design space for CC and FTV control effectors is illustrated schematically in Fig. 2. Note that the slot design for both CC and FTV is driven by the requirement that the external flow remains attached to the surface up to the slot lip. This means that the slot lip must be located on the CC trailing edge or reaction surface at a point where the surface tangent is parallel to the external flow immediately upstream of the slot. As such, there is little design freedom to vary this location and it is not considered as a design variable in this study. In order to focus attention on the core design process rather than design details, the CC method presented here assumes the application is for a straight, unswept wing. In practice, the design method can be applied to arbitrary planform geometries using a strip theory approach[17] as long as the flow over the wing can be assumed to be approximately two dimensional. Note that method relies on prediction of delta C_L hence is applicable to low aspect ratio wings where the spanwise load distribution is non uniform as long as the flow remains two dimensional.

2.2 Circulation control design variables

The design objective for the CC system is defined by a roll manoeuvre specification that must be met with minimum overall cost to the aircraft. The installed drag penalty is primarily a function of the trailing edge radius to mean aerodynamic chord ratio. Early CC systems for high lift tended to have a relatively large R_{cc}/c ratio, e.g. 3·7%[18], and hence incurred a significant drag penalty. Hoerner[19] shows that for a range of airfoils including NACA 4-series, as the thickness of a squared off (blunt) trailing edge is reduced, the profile drag coefficient also reduces. However, if the trailing edge is thinner than roughly half the local boundary layer thickness, then the drag will be similar to that of sharp trailing edge. There is little published data detailing the effect of a round trailing edge on the profile drag of a wing; however to a first approximation it is a reasonable to assume that for drag estimation purposes that the equivalent thickness of a curved trailing edge is equivalent to twice the radius. Note that if the increase in base drag is unacceptable, employing low blowing through both CC slots reduces trailing edge separation and produces a localised thrust, countering the drag increase[20].

The installed volume of the actuator is primarily due to the requirement for a suitable plenum ahead of the CC slot, with the plenum acting as a geometric interface between a circular air inlet pipe and a high aspect ratio rectangular slot exit. The plenum design objective is to reduce the total pressure distortion at the slot exit at the same time as reducing plenum volume and the pressure drop across the plenum. The total pressure distortion metric is defined here as the standard deviation of slot exit total pressure nondimensionalised by the mean slot exit total pressure:

$$\tilde{p} = \sigma_{p0}/\overline{P_o} \qquad \ldots (1)$$

With reference to the geometry defined in Fig. 2, the required plenum volume is determined by the plenum contraction ratio and plenum aspect ratio, where

$$\text{Plenum contraction ratio} = CR_p = H_{cc}/h \qquad \ldots (2)$$

and

$$\text{Plenum aspect ratio} = AR_p = b_{cc}/d_{cc} \qquad \ldots (3)$$

To a first approximation, the plenum contraction ratio determines the ratio of the velocity of the air at plenum entry to the velocity at the plenum exit, and hence the static pressure gradient between plenum entry and exit. This static pressure gradient is favourable in the sense that it reduces the boundary layer growth on the plenum walls to produce the desired 'top hat' velocity profile, and also tends to reduce spatial and temporal variations in the jet velocity that promote turbulent break-up of the jet sheet. As a rule of thumb, it is usual to use a plenum contraction ratio of at least ten for plenums used for laboratory experiments. From simple application of continuity and the isentropic flow relations, the use of a contraction ratio of 10 implies that the static pressure in the plenum will be equal to 99% of the total pressure of the flow, thus providing a simple means of determining jet exit velocity from single static pressure reading.

The plenum aspect ratio is important from a fluid dynamics perspective because, for the usual case of a central circular plenum inlet, it determines the degree of flow spreading required to get uniform total pressure along the slot exit. For a high aspect ratio plenum, the flow spreading angle is high and it is likely that without correction, the exit total pressure opposite the plenum entrance will be higher than at the edges. From an implementation perspective, for a given spanwise extent b_{cc} of a CC slot, the plenum aspect ratio determines the chordwise extent of the CC unit. In order to reduce implementation cost, this should be reduced, i.e. the plenum aspect ratio should be increased, which conflicts with the requirement for good total pressure uniformity. In the present work, the goal has been to replace conventional hinged surfaces and the existing space for these surfaces has been replaced with a plenum without trying to reduce the chordwise extent.

If the plenum contraction ratio is low and the aspect ratio is high then it is still possible to achieve good uniformity of total pressure at the slot by introducing a gauze or baffles within the chamber. These create a pressure drop in the flow and hence a higher supply pressure is needed to achieve the same jet exit velocity. This cost is represented by a plenum efficiency metric, defined as the ratio of outlet total pressure to inlet total pressure:

$$\eta_p = \frac{P_{o,o}}{P_{o,i}} = \frac{q_j}{P_{o,i}} \qquad \ldots (4)$$

For a given plenum geometry, the total pressure uniformity at the slot exit also depends on the geometric tolerances of the slot itself. Slot geometric distortion is defined here as the standard deviation of the slot height divided by the mean slot height:

$$h = \frac{\sigma_h}{\overline{h}} \qquad \ldots (5)$$

Slot total pressure uniformity is increased by increasing the slot geometric uniformity, however there is a design and manufacturing cost associated with decreasing slot tolerances and it becomes increasingly expensive to maintain a given slot geometric uniformity as the mean slot height decreases.

Attention will now be focused on the costs associated with provision of pneumatic power for actuation. Fluid power is the product of volume flow rate and pressure and a given power source will have a performance map that defines the limits over which flow and pressure can be varied. Because of this, efficiently matching flow control actuators with a power source is a non trivial engineering task. If air is bled from the compressor stage of a gas turbine engine, then the pressure available is typically well in excess of the typical maximum delivery pressure ratio of around two (sonic exit conditions) needed for fluidic control applications. Because of this, the main power system constraint is mass flow rate availability and, as such, the primary PPS design objective for fluidic controls is the minimisation of mass flow.

For a given control location on a vehicle, the amount of mass flow required for a given manoeuvre specification is primarily defined by the fluidic gain of the control,

https://doi.org/10.1017/S0001924000003365 Published online by Cambridge University Press

$$a_{cc} = \frac{dC_L}{dC_\mu} \quad \ldots (6)$$

where the momentum coefficient is defined as

$$C_\mu = \frac{\rho A_j U_j^2}{q_\infty S} = \frac{m U_j}{q_\infty S} \quad \ldots (7)$$

Note that the momentum coefficient depends on the product of the slot mass flow rate and the jet velocity. Given the likelihood that the PPS will be mass flow limited rather than pressure limited, it can be seen that for mass flow efficiency the slot design should be driven towards using the highest jet velocity possible. In practice, at jet Mach numbers greater than unity, compressibility effects limit the degree to which the jet will remain attached to a curved surface and the aerodynamic gain reduces towards zero. However, the Mach number at which critical degradation of performance occurs depends on the slot curvature (see discussion below), so the design choice is not simple.

The aerodynamic gain defined above represents the number of units of force obtained per unit of momentum input, and for a well implemented system values of the order of 50 are achievable[21] at low blowing rates. At higher blowing rates consistent with levels of effectiveness required for flight control, a more typical value of gain is around ten. The overall efficiency depends both on the aerodynamic gain of the control and the mass cost of the systems required to deliver the appropriate mass flow to the control; these systems effects are discussed in Section 5. Given a well designed plenum system delivering a uniform total pressure at the slot exit and a subcritical jet Mach number, the control gain is increased by reducing the dimensionless slot curvature

$$C_h = \frac{h}{R}. \quad \ldots (8)$$

For a given slot spanwise length, decreasing h also decreases the slot area, which has the favourable effect of reducing the mass flow required for a given momentum coefficient as discussed above.

Experimental evidence[22] suggests that good performance is obtained for a dimensionless slot curvature of around 0·05 or less. Given the requirement to reduce the trailing edge radius to reduce drag, an efficient design is driven towards using very small slot heights. Note that this reinforces the design driver for reducing slot height to reduce mass flow for a given C_μ discussed above. In practice, however, as h becomes very small it becomes increasingly costly to maintain slot geometric uniformity leading to practical lower limits on slot height. The specific lower limit on slot height depends on the application in hand; however slot heights of the order of 0·1mm would appear to represent a practical limit based on anecdotal evidence.

2.3 Fluidic thrust vectoring design variables

Noting the similarities between the CC and FTV geometry, the design variables for FTV are similar to those for CC described above. As such, this subsection will focus mainly on the design differences between the two systems.

For an FTV system, the performance requirement is defined by the vehicle longitudinal trim and pitch manoeuvre specification. The process of turning this into an FTV requirement is non-trivial due to the fact that the control force obtained depends both on the direction and magnitude of the thrust vector, and that the thrust magnitude varies with flight condition. The most challenging case is typically trim at C_{Lmax} for landing. Here, the required control force is a maximum; however the thrust magnitude is typically a minimum. This condition will typically define the termination angle, θ_T, of the reaction surfaces (note that for the CC configuration with a circular trailing edge, the termination angle is effectively 180°). The choice of reaction surface radius for an FTV system is still driven by the need to increase fluidic gain by reducing slot curvature, however, in this case, it is the dimensionless curvature of the primary jet

$$C_{hp} = \frac{h_p}{R_{FTV}} \quad \ldots (9)$$

that drives the fluidic gain. The fluidic gain for FTV is defined as;

$$a_{FTV} = \frac{F_Z}{\rho A_P U_P^2} = \frac{C_z}{C_{\mu FTV}}. \quad \ldots (10)$$

In order to reduce the primary slot curvature, the propulsive nozzle should have a high aspect ratio $\left(\frac{b_{FTV}}{h_p}\right)$ such that the nozzle slot height is minimised for a given cross sectional area. Note that low observable considerations also drive nozzle exits to be high aspect ratio 'letter box' designs, providing favourable design convergence.

The installation drag penalty from FTV comes from the increased base area due to the implementation of reaction surfaces. From geometry, the ratio of projected reaction surface area in the *yz* plane to nozzle area is

$$\text{Nozzle Area} = \frac{2(1 - \text{Cos}\theta_T)}{C_{hp}} \quad \ldots (11)$$

Base drag is thus reduced by having a high primary slot curvature and a small reaction surface termination angle. This drives the design towards being ineffective and inefficient, respectively, and hence appropriate design trade studies need to be considered.

The plenum geometry metrics devised for the CC system and the advantages of minimising the (secondary) slot height are equally applicable to FTV and hence require no further discussion.

2.4 Design methodology for CC and FTV

Flow charts representing a design methodology for CC and FTV are shown side by side in Fig. 3. The figure is intended to give a broad view of the key steps in the design process and to highlight the engineering decision making process. The design methodology has been cast such that the 'output' at the bottom the design cycle is the required mass flow. This arrangement was chosen on the basis that for subsonic gas turbine powered flight vehicles mass flow requirement is likely to be the key design driver for fluidic controls.

From the discussion in the previous sections, it is clear that the design process for each of the fluid controls will be similar. The most important difference is due to the fact that fluidic gain for the CC system is driven by the dimensionless curvature of the control jet whereas for FTV, the gain is driven by the dimensionless curvature of the jet flow adjacent to the control jet. Furthermore, the drag penalty associated with CC can be driven down to almost zero whilst retaining an efficient system, whereas the base drag from an efficient and effective FTV system will probably be a significant cost that has to be mitigated against overall benefits. This makes the design process for FTV more challenging than for CC.

3.0 APPLICATION – CASE STUDY

3.1 Introduction

The design methodology developed above was applied to the design of fluidic flight controls for the DEMON demonstrator aircraft being developed for the UK EPSRC/BAE Systems funded FLAVIIR research programme[23]. The stated goal of the flight demonstration is successful completion of a complete flight cycle without use of moving surface controls.

https://doi.org/10.1017/S0001924000003365 Published online by Cambridge University Press

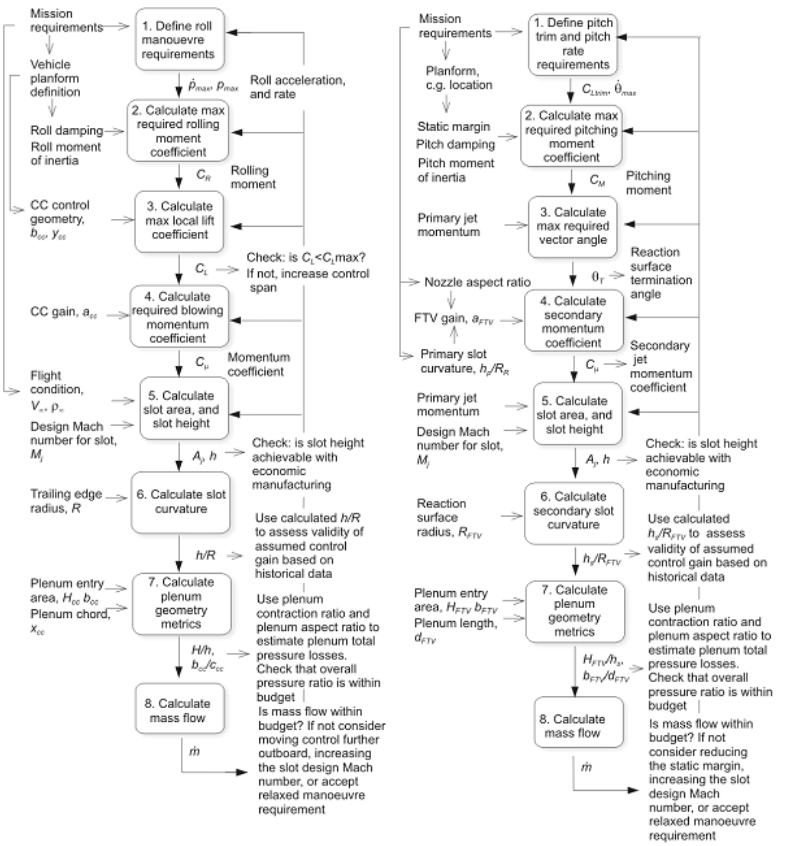

a) Circulation Control b) Fluidic Thrust Vectoring

Figure 3. Low order design methodology for fluidic flight controls.

The basic specification of the DEMON aircraft and location of the fluidic controls is shown in Fig. 4. The DEMON aircraft planform and internal structure is based on a scaled version of an earlier aircraft known as Eclipse, and it was specified that the CC units for roll and pitch control should fit within the geometric boundaries of the existing moving control surfaces. Two options were open for the aircraft PPS: either use of engine bleed or bleed from a dedicated APU.

Sizing of the CC and FTV fluidic controls in terms of the required air mass flow/pressure and slot area was conducted according to the process shown in Figs 3(a) and (b). The sizing process for both CC and FTV broadly follows the same three main steps: first the relevant vehicle performance requirement is expressed in terms of the maximum control moment coefficient required. Second, this moment is converted into a required momentum coefficient using historical understanding of typical achievable control gains, and third, a valid slot geometry is defined that is able to deliver the required momentum whilst meeting requirements for control efficiency and effectiveness, and manufacturing constraints. The data used to inform the sizing process comes from various sources, including subscale wind tunnel experiments[6,18,21,24,25], data sheets[26-28], 1d flow pipe simulation[29], theoretical analysis[14,21,24,30] and heuristics based on previous successful flow control implementations[3,7,14,15,24,31-35].

Given a slot area and slot height defined at stage five in the process, the next major undertaking was translating these requirements into practical flight hardware and this will be covered in the next section. Hardware development for the CC system will be considered first, followed by the FTV hardware second.

3.2 CC hardware design

Geometric details of the final design solution developed for the CC units are shown in Fig. 5. The main features of the unit design are summarised in Fig. 5(a). The key design objective is the controlled delivery of thin, uniform jets of air immediately above and below a curved trailing edge with the trailing edge geometry having minimal aircraft drag penalty compared to a sharp trailing edge. The estimated thickness of a turbulent boundary layer at the trailing edge of the mean aerodynamic chord (length 1·5m) at a cruise speed 45ms^{-1} at sea level conditions based on flow over a flat plate is around 26mm. The diameter of the trailing edge in the present design is 6mm, i.e. around 0·23δ, which is less than the 0·5δ criteria identified in Section 2.2. Hence it is anticipated that there will be no significant drag penalty associated with using a curved trailing edge on the CC control compared to a sharp trailing edge.

Figure 5(b) shows a cross section through the CC unit and identifies the main structural design features. The CC unit is symmetric about the horizontal centreline with compressed air for the upper and lower plenums delivered through pipes entering the right bulkhead of the unit. The unit is attached to the rear spar of the aircraft by bolting through this bulkhead. The left hand side of the unit comprises the trailing edge of the wing and consists of a cylindrical section that forms a Coanda surface for the upper and lower slots. The upper and lower plates of the unit are held rigidly in place by screws into plenum support pillars.

The arrangement for achieving precise control of the slot height is shown in Fig. 5(c). A key feature of this design is that the slot height is set by provision of slot spacers machined into the plenum divider,

https://doi.org/10.1017/S0001924000003365 Published online by Cambridge University Press

with the plenum upper and lower plates are maintained in compression against these slot spacers by slot tensioning screws. This allows relative movement between plenum outer plates and the slot spacers and avoids the generation of compressive stresses in the plates in this region due to thermal expansion, pressure loads or wing bending. Since the plates are rigidly fixed to the plenum via the slot tensioning screws the actual relative motion between the plates and slot spacers is likely to be very small; however provision of this local degree of freedom may be critical in preventing slot distortion under normal operating conditions.

A close-up of the CC unit trailing edge is shown in Fig. 5(d). The geometry defined here is critical to the aerodynamic efficiency and effectiveness of the CC device and needs to be controlled precisely. The key features are:

1) The plenum contraction continues all the way to the slot slip, minimising the boundary height at the jet exit and avoiding problems due to local unsteady separation upstream of the slot exit (slot burble)
2) The contraction profile up to the slot lip is linear and symmetric top and bottom. This reduces the amount of skew in the velocity profile at the jet exit plane
3) The jet centreline is exactly tangential to the curved trailing edge at the exit plane of the slot. This ensures proper initial attachment of the jet to the Coanda surface. Incorrect alignment of the jet exit with respect to the Coanda surface can result in complete failure of the jet to attach and hence failure of the desired control function.
4) The slot lip thickness is reduced to as thin as practical manufacturing and handling constraints allow (0·5mm), though ideally this should be of the same order or smaller than the slot height of 0·2mm.
5) The slot spacers terminate before the slot lip. This reduces the impact of the total pressure deficit downstream of the spacers by allowing redistribution of flow total pressure prior to jet sheet formation. If the spacers go all the way to the slot lip then the resulting jet sheet typically splits into a number of smaller cells defined by the slot spacers.

A plan view of the CC unit is shown in Fig. 5(e). This figure illustrates the relative frequency and spacing of the slot spacers and slot tensioning screws and also shows the division of the trailing edges of the upper and lower plenum plates into a number of tabs or 'fingers' via thin slots filled with a flexible sealant. Note that for reasons of convenience the design shown in these figures is for an unswept trailing edge. In the swept version, the slot fingers are aligned in the streamwise direction, however the slot spacers remain normal to the trailing edge. The provision of a fingered trailing edge performs two important roles. Firstly, the compression of each of these fingers against the slot spacers can be adjusted independently of their neighbours. This allows precise control of the slot compression and compensation against uneven loading. Secondly, the provision of flexible spanwise gaps in the slot lip allows relief of spanwise compressive stresses in the slot lip that would otherwise cause buckling or waviness in the trailing edge. Whilst the slot spacers are repeated every 10mm, the slot height of 0·2mm is only 2% of this spacing and hence care must be taken to ensure maintain the desired slot geometric uniformity.

3.3 FTV hardware design

Attention is now focussed on the design of the FTV hardware, Fig. 6. An isometric view of the overall nozzle assembly is shown in Fig. 6(a). The primary nozzle jet pipe is a rectangular section duct that blends from a square inlet to a rectangular outlet with aspect ratio 10 and area 4,410mm^2. The duct outlet area is 95% of the inlet area with a linear area blend as recommended by the engine supplier. The FTV unit is a collar assembly that sits around the exit of the primary

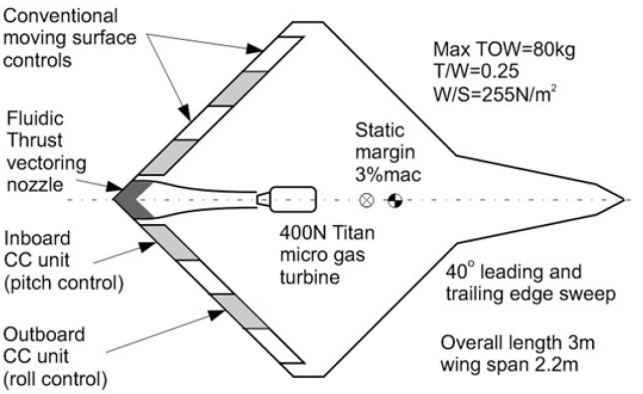

Figure 4. Overview of the DEMON UAV highlighting the location of conventional and fluidic flight controls.

nozzle, and provides upper and lower reaction surfaces and upper and lower plenums for the secondary control jets. The jet pipe is made from welded 1mm titanium sheet, whereas the FTV unit is machined from titanium billet.

Key geometric features of the FTV unit are shown in a vertical cross section parallel to the centre line of the nozzle, Fig. 6(b). The design of the FTV plenums is similar to that of the CC unit plenums, with the upper and lower halves of each plenum being pressed together to form an exit slot whose height is determined by a number of slot spacers (Fig. 6(d)).

A vertical cross section through the FTV nozzle normal to the swept exit plane of the nozzle is shown in Fig. 6(c). This section forms the aerodynamic design case for the FTV unit on the basis that from geometric considerations, it is only the flow component normal to the nozzle exit plane that is vectored (the flow component parallel to the nozzle exit plane is essentially unaffected by the presence of the reaction surfaces since the reaction surfaces induce no flow curvature in this plane). The primary nozzle curvature was specified as 0·2 based on experience from other FTV studies[14,15]. Given a primary jet slot height of 20mm, this gives the required reaction surface radius as 100mm. From vehicle longitudinal trim and manoeuvre considerations, the target maximum deflection angle of the primary jet was defined as 20°. Based on experience, this translated into a required reaction surface termination angle of 35° (in practice, spreading of the jet means that when the jet is fully attached to a reaction surface, the vector angle of the jet centre line is always less than termination angle of the reaction surface). The secondary slot height is 0·25mm, giving a secondary slot curvature is 0·0024. The relatively low value of secondary slot curvature compared to the slot curvature for the CC unit (0·070) means that in principle adequate Coanda attachment of the secondary jet can be achieved with relaxed slot geometric and total pressure distortion levels compared to those for the CC unit[36].

The detailed design of the slot lip area is shown in Fig. 6(d). The geometry here is designed in a similar way to the CC unit slot lip, with the secondary slot height being set by slot spacers machined from the wall of the primary nozzle. The other side of the spacer is held in compression against the wall of the secondary nozzle and has limited ability to translate on this surface in response to thermal or mechanical loads on the nozzle and hence has a reduced tendency to buckle under thermal or pressure loads. Unlike the CC units, the FTV nozzle does not feature slot tensioning screws or slot fingers due to the practical difficulties of implementation for the nozzle case.

A plan view of the FTV nozzle assembly is shown in Fig. 6(e). The nozzle trailing edge is swept at the same angle as the trailing edge of the wing (40°). Note that the undeflected primary jet exits the primary nozzle in a direction parallel to the nozzle centre line, whereas the secondary jets exit the secondary nozzles normal to the

https://doi.org/10.1017/S0001924000003365 Published online by Cambridge University Press

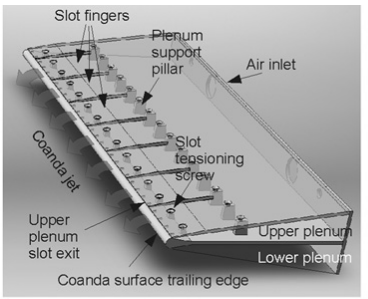

a) Isometric view of CC unit assembly

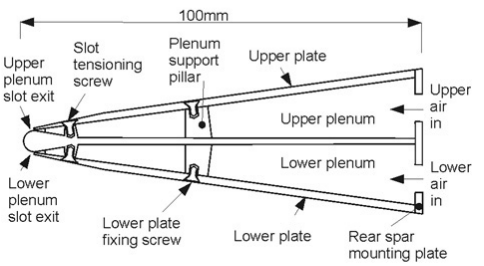

b) CC unit cross section

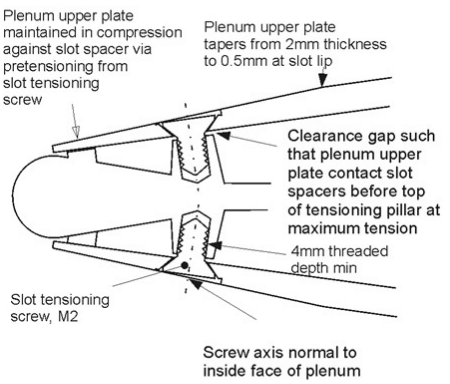

c) Slot tensioning arrangement

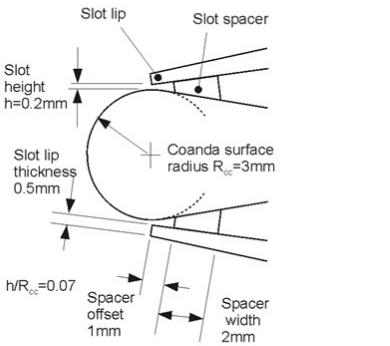

d) Definition of slot exit and Coanda surface geometry

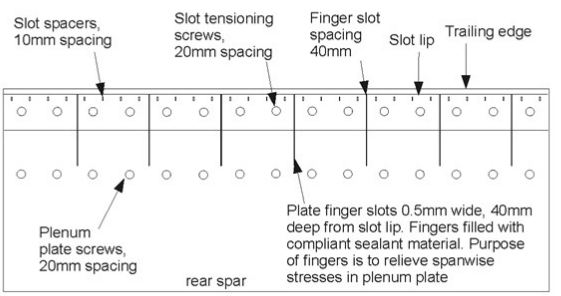

e) Plan view of CC plenum

Figure 5. CC design for DEMON.

slot lip. The reason for this, as mentioned above, is that it is the component of primary jet momentum normal to the nozzle exit plane that is vectored and hence this defines the direction in which the secondary control momentum should be injected to achieve maximum efficiency. Note that from the aforementioned geometric considerations, vectoring using swept reaction surfaces introduces both a pitch and yaw component to the resultant jet. For a nozzle with a forward swept trailing edge (negative sweep angle) as shown in Fig. 6(e), positive or negative vectoring in pitch of one half of the jet either side of the nozzle centre line will also result in the jet vectoring towards the centreline, i.e. a side force in a direction away from the nozzle centreline. For an aft swept trailing edge the direction of the side force is reversed. For example, for a nozzle on the port side of the aircraft with a sweep angle of –45° and jet deflection angle of 30° up in a vertical plane normal to the nozzle exit plane, the resulting thrust components in the aircraft body axes will be +5 units of vertical (z direction) force and –1 unit of side force (y direction). For the case of the DEMON nozzle, the nozzle has left-right mirror symmetry about the aircraft centre line and the secondary blowing is the same on both sides, hence the side forces generated on each side of the nozzle cancel out leaving a pure normal force. The inherently skewed nature of vectoring from swept reaction surfaces raises interesting questions on how the three dimensional geometry of FTV nozzles should be defined. The current nozzle configuration is geometrically simple, but is unlikely to be optimal.

It is recognised that there are some losses in propulsive efficiency due to modifications to the nozzle and jet pipe necessary for implementation of FTV. Section 2.3 discusses the impact of the reaction surfaces on base drag, however there may also be effects due to the presence of an effectively divergent diffuser section downstream of the primary nozzle exit. This issue does depend on the design pressure ratio for the nozzle, however if the primary flow can be made to separate cleanly at the slot lip (no attachment to the reaction surfaces) e.g. by using a small amount of secondary blowing, then initial analysis indicates that the loss in propulsive efficiency due to the presence of the reaction surfaces is small compared to other losses in the propulsion system. The design of FTV systems for supercritical nozzle applications presents different challenges and is outside the scope of the present work. The use of a jet pipe with a

https://doi.org/10.1017/S0001924000003365 Published online by Cambridge University Press

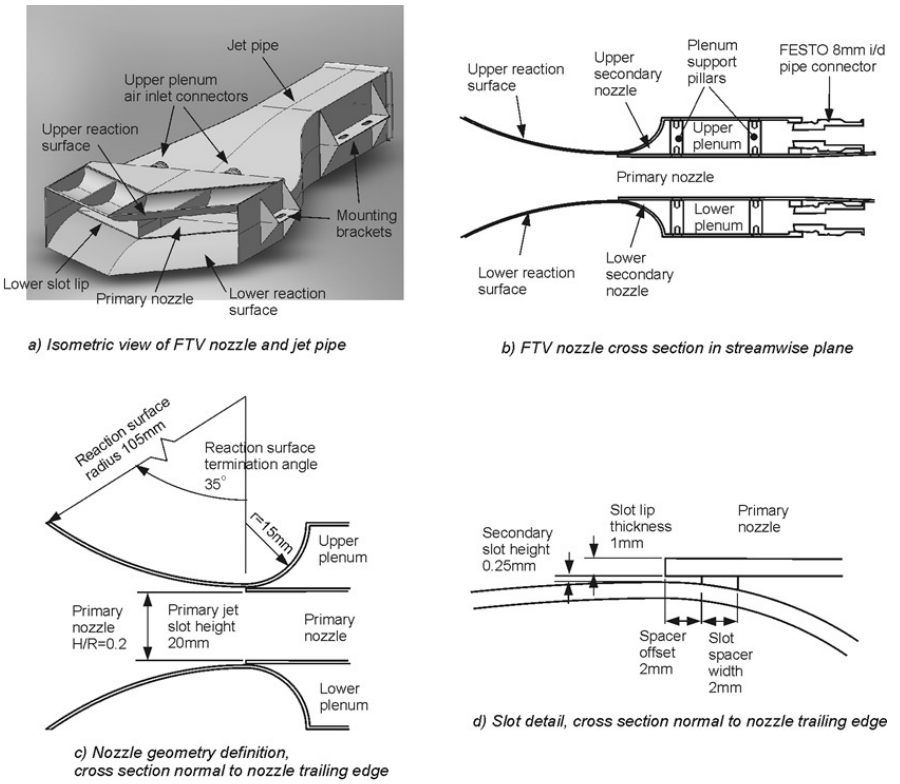

Figure 6. FTV design for DEMON.

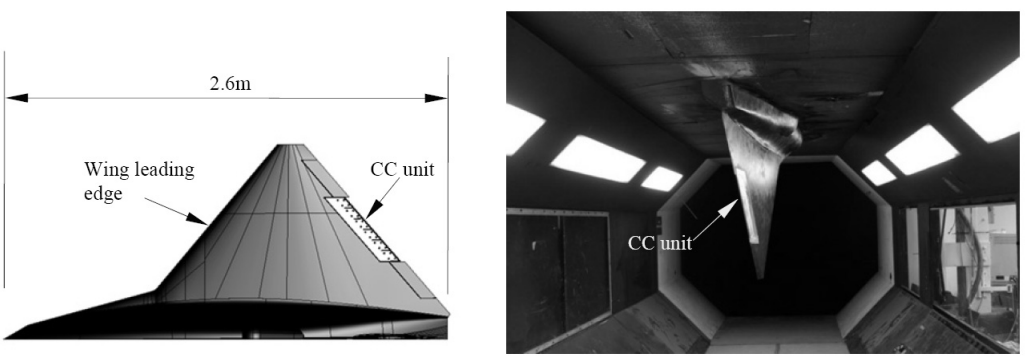

(a) Plan view of DEMON half model showing location of CC unit

(b) Rear view of DEMON half model mounted on the overhead balance in 2·1 x 2·7m wind tunnel

Figure 7. CC wind-tunnel test on DEMON half model.

https://doi.org/10.1017/S0001924000003365 Published online by Cambridge University Press

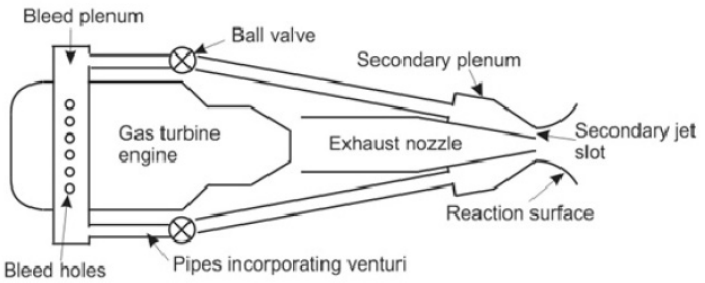

a) Rig schematic showing nozzle configuration and engine bleed system.

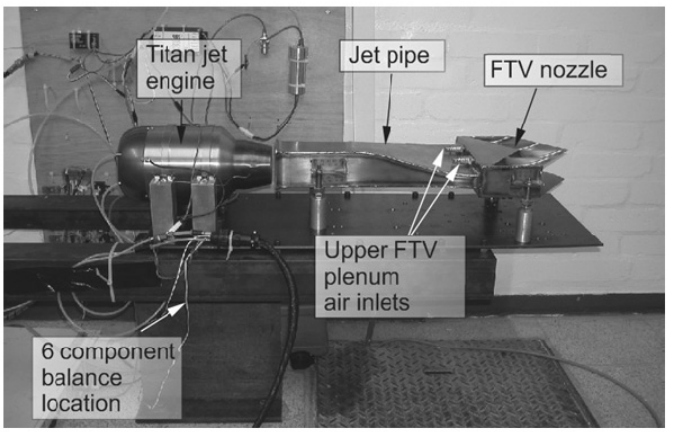

b) Test rig photograph. Configuration shown here is without engine bleed system installed.

Figure 8. FTV experimental rig.

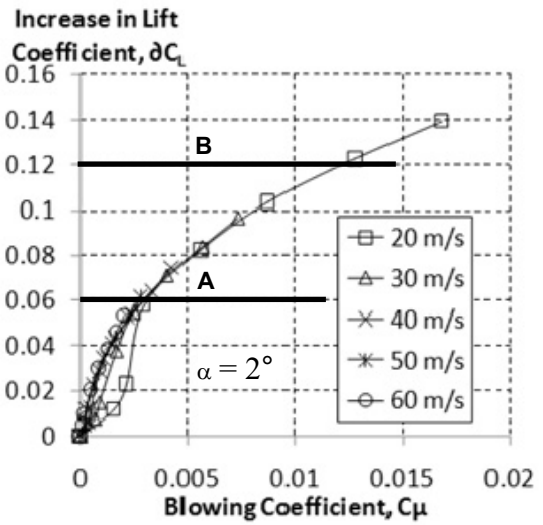

a) CC lift curve at varying free stream speeds

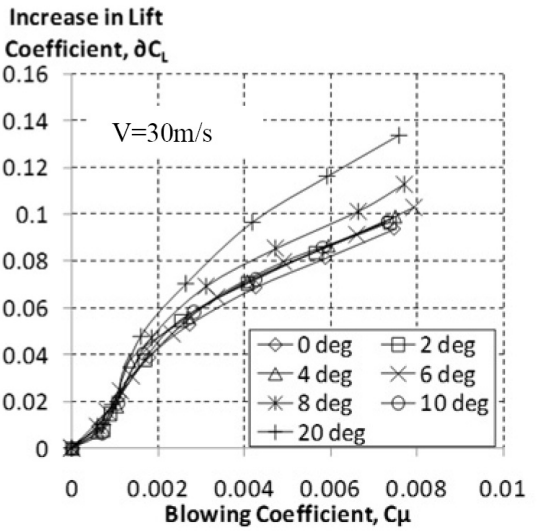

b) CC lift curve at varying incidence

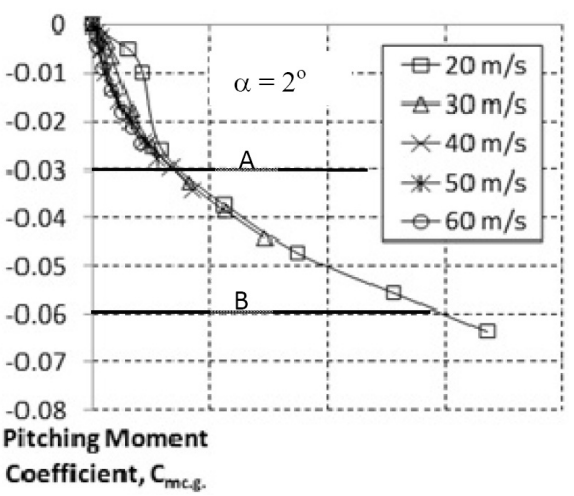

c) CC pitching moment characteristic at varying free stream speeds (same Cμ scale as a))

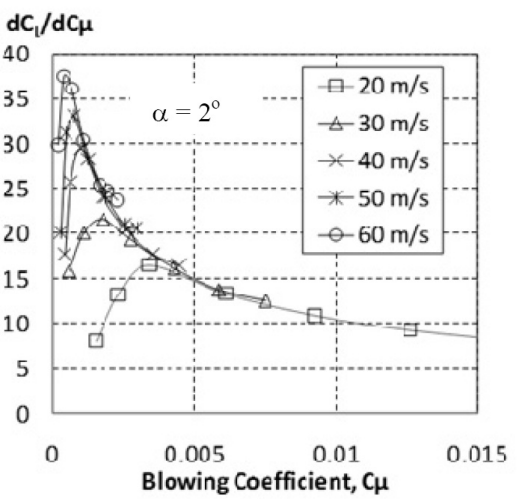

d) CC gain for varying free stream speed (same case as shown in a))

Figure 9. Selected wind tunnel results demonstrating the control performance of a CC manoeuvre effector on the DEMON aircraft. For reference, line A in subfigures a) and c) represents the control response magnitude from 30° deflection of an inboard elevon and line B indicates the control response magnitude from 30° deflection of both an inboard and outboard elevon.

https://doi.org/10.1017/S0001924000003365 Published online by Cambridge University Press

circular inlet and letterbox exit compared to a uniform circular pipe introduces additional total pressure losses and an increase in nozzle weight. CFD analysis on the present jet pipe geometry by Sobester[37] showed that pressure losses could be reduced to 4% with careful design (compared to typical pressure losses for a circular jet pipe of around 2%). With regard to nozzle structure weight, Burley determined a relationship between nozzle weight and aspect ratio and calculated that a nozzle with AR = 10 was ~1·6 times heavier than a circular nozzle[38]. Further discussion of propulsive efficiency and weight effects due to the addition of FTV capability to a nozzle are discussed by Gill[14].

4.0 EXPERIMENTAL EVALUATION OF FLUIDIC CONTROL PERFORMANCE

This section provides a brief evaluation of the performance of the CC and FTV units designed for the DEMON aircraft to provide closure on the design methodology proposed in this paper. More detailed experimental data may be found in references[14,24].

A CC unit based on the design shown in Fig. 5 was fitted into the trailing edge of an 85% scale half-span model of the DEMON aircraft, Fig. 7. This CC unit was an early prototype and only had a single blowing slot on the upper surface of the trailing edge. The DEMON model was mounted on the overhead balance in the 2·1m x 2·8m closed return wind tunnel at the Goldstein Research Laboratory at the University of Manchester. This tunnel has a maximum velocity of 70ms^{-1} in the working section and free stream turbulence levels of 0·5% at 20ms^{-1}. The pneumatic power supply for the CC effector was provided by ducting air into the model from an external tank. The pipes were relatively flexible and were arranged such that tare effects due to pressurisation were minimised. The air flow rate was regulated by a servo driven butterfly valve. The experimental independent variables were CC plenum pressure (0-1·4bar), model angle of attack (0-20°) and free stream speed (20-60ms^{-1}). The dependent variables were CC mass flow (measured using an inline Venturi meter), and six components of force and moment from the wind tunnel balance. The measurement of both plenum pressure and mass flow improved the accuracy of the slot momentum flow calculation by removing the need to know the slot area, which in practice is subject to a high degree of measurement uncertainty if determined from geometry.

The FTV rig consisted of an FTV nozzle and micro gas turbine engine mounted to a base plate, with the base plate connected to earth via a six component strain gauge balance. The FTV plenums were supplied with compressed air bled from the outlet of the engine centrifugal compressor. Upper and lower plenum pressure was regulated via manually operated ball valves in the supply lines. A photograph of the set up is shown in Fig. 8. Further details on the design of the engine bleed system may be found in Gill[31]. Note that a significant motivation for using an engine based test rig is that balance tare effects due to transporting high momentum flows across the balance earth are avoided and hence accurate measurements of forces and moments can be obtained with a relatively simple test set up. Use of an engine also provides representative thermal stressing of the nozzle assembly during operation and hence exposes potential problems due to nozzle geometric distortion. These benefits are set against the operational challenges of using micro gas turbines as part of an experimental set up.

A sample set of results from the CC unit tests are shown in Fig. 9. Figures 9(a) and (b) illustrate the fundamental control response of the device in terms of the change in lift coefficient with blowing momentum coefficient, with Fig. 9(a) showing the effect of varying free stream speeds at fixed angle of attack and Fig. 9(b) showing the effect of varying angle of attack for fixed free stream speed. The data collapses reasonably well for both these cases confirming that the forces and moment coefficients scale as a function of velocity ratio. The amplification gain as a function of blowing coefficient is

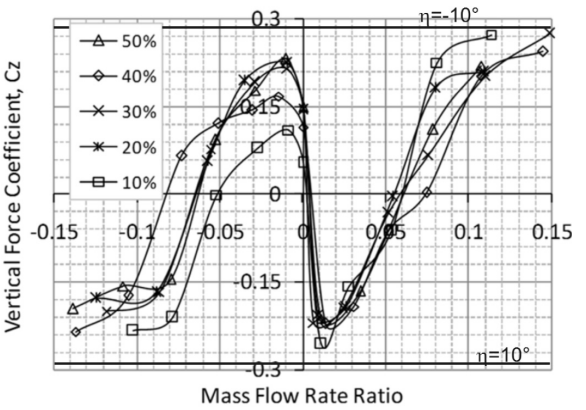

(a) FTV control response curves for varying engine throttle setting. The 'N' shaped response is made up of a 'reverse' control region at low blowing rates coupled with a 'forward' control region at high blowing rates. The vertical force coefficient obtained from a 10° elevator deflection on the DEMON aircraft is shown for reference (elevator comprised of the two innermost control surfaces on Fig. 4 for each wing).

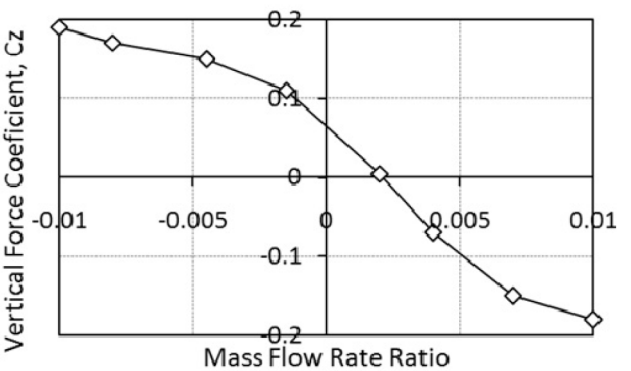

(b) Example FTV control response at low blowing rates ('reverse control' region of Fig. 10(a)).

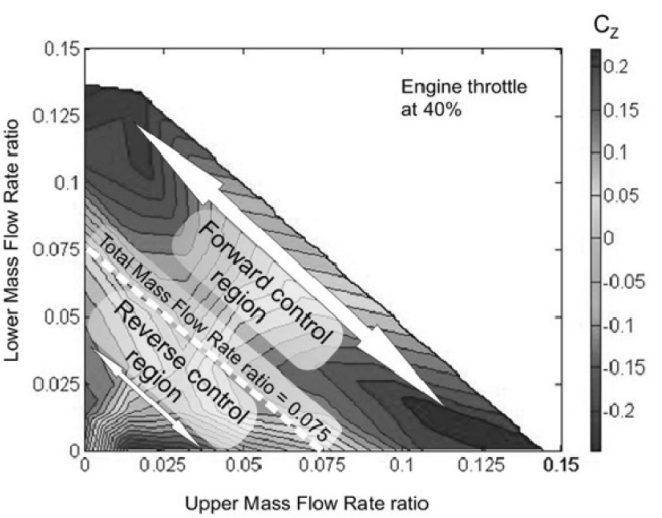

c) FTV control map for combinations of upper and lower slot blowing. White arrows indicate possible control schemes based on constant total blowing from both slots. Control in the reverse region uses up to 10 times less air than in the forward region for the same control effectiveness.

Figure 10. Example FTV experimental results illustrating the two distinct control response regions. The control gain in the reverse region is up to a factor of 10 greater than in the forward region.

https://doi.org/10.1017/S0001924000003365 Published online by Cambridge University Press

shown in Fig. 9(d). As the blowing coefficient reduces to zero, the gain asymptotes towards to a value of around 40. The increased gain at low blowing rates is usually attributed to the CC initially acting as a boundary layer control device[39], however the physical basis of this assertion remains open to question. At a blowing coefficient of 0·01, the lift increment is just over 0·1, giving a gain value of around 10. This operating condition is consistent with a maximum control input that might be used in practice and corresponds to bleeding approximately 10% of engine mass flow during the cruise condition. The rolling moment produced at C_μ = 0·001 equates to a 10° aileron lateral asymmetric deflection on the same vehicle[40]. In a NASA study by Fears *et al*. investigating stability and control characteristics on swept bodies, a delta planform with 50° LE/TE sweep and a wide body (most applicable to DEMON) obtained a $\Delta C_L = \pm 0{\cdot}1$ for a flap deflection of ±30°[41].

The rolling moment obtained from the CC device (not shown here) follows identical form to the lift coefficient response. This is consistent with the strip theory modelling approach by which rolling moment is calculated by taking the product of the lift increment at a particular spanwise station and the radius arm of this station from the centre of gravity. The pitching moment about the centre of gravity obtained from the CC is shown in Fig. 9(c). This is again of similar form to the lift coefficient response as expected, with a negative slope due to the centre of gravity being ahead of the wing aerodynamic centre. The significant pitch response of the CC device confirms that when used for roll control, a pair of CC devices both with upper and lower surface blowing must be used in a similar manner to conventional ailerons in order to cancel out any control induced pitching moments.

A sample set of results from the FTV rig is shown in Fig. 10. Consider the control response curves first, Figs 10(a) and (b). The abscissa in these plots is the mass flow ratio, defined as the ratio of the secondary jet to mass flow to the primary jet mass flow. The mass flow ratio has been used here instead of the momentum coefficient because the main engineering constraint on an engine bleed based system is the percentage engine bleed available for control (typically around 20% for a simple micro gas turbine engine at full thrust, but decreasing with reducing throttle[31]). Positive mass flow ratio corresponds to blowing from the upper plenum and negative mass flow corresponds to blowing from the lower plenum. The ordinate for the control response curves is the nozzle normal force coefficient C_Z, defined as the ratio of the nozzle normal force to the primary jet momentum. From geometry, the vector angle of the primary jet δ is given by $\mathrm{Sin}\delta = C_z$. As a reference, a C_z value of 0·3 corresponds to a vector angle of approximately 17°. C_z produced by a 10° elevator deflection is shown on Fig. 10(a) for reference; the elevator in this case is the two innermost control surfaces on either wing, shown in Fig. 4.

The full range FTV control characteristic (figure 10(a)) has a distinct '*N*' shaped profile with a positive slope at high mass flow ratios but a negative slope at low mass flow ratios, with the control reversal occurring at around a mass flow ratio of 0·01. Operation in the negative slope region of the control response is referred to as to 'reversed control', whereas operation in the positive slope region is referred to as 'forward control'. Other experimental data not shown here suggests that the critical parameter determining when the control reversal happens is the Mach number ratio between the primary and secondary jets, with the crossover happening at a Mach number ratio of around 1. Based on data not shown here, the FTV (momentum) gain given by $a_{\mathrm{FTV}} = \dfrac{C_Z}{C_{\mu FTV}}$ is found to be around 30 in the reverse control region and around three in the forward control region. This is a significant difference and hence the preferred mode of operation from an efficiency point of view is the reverse control mode[14].

Figure 10 shows a contour plot of the FTV control response to combinations of both upper and lower slot blowing (dual blowing). The data in Figures 10(a) and b) is subset of this data obtained by taking values from a locus made up of the *y* and *x* axes only. Loci parallel to the *-yx* direction correspond to lines of constant total secondary mass flow, i.e. the sum of the mass flow from the lower and upper slots is a constant. Referring to Fig. 10(a) it can be seen that the control response is reversed between a mass flow rate ration of around +/– 0·075. From Fig. 10(c) it can be seen that dual blowing at a combined rate above 0·075 means that the control response is always in the forward direction. However, as mentioned above, the efficiency here is low and hence there is a strong incentive to use the reverse control region. There were some concerns initially that the high gain in the reverse control region would lead to a problematic control response, e.g. tendency to bistable behaviour. However, in practice, it is found that as long as control valves are appropriately sized for the mass flow range of interest, then the control response is sufficiently linear for use as part of a flight control system[14].

Whilst there was no sign of static hysteresis in the present experiments, other unpublished data taken on similar nozzles in the same lab has shown that hysteresis does occur if the slot step height (slot lip thickness + secondary slot height) to reaction surface radius becomes small. Since decreasing his parameter also increases the gain of the system, the onset of static hysteresis places an upper limit on the achievable gain from this type of FTV system.

A further practical issue concerns the time response of both the CC and FTV systems. The time response of the present pneumatic controls is made up of three components: the time take for the control valve to open, the time taken for the jet at the slot exit to reach steady state following valve opening, and the time the outer flow takes to adjust to the change in boundary condition created by the jet. This latter aerodynamic delay is of the same order as would be expected for conventional flapped controls and is based on the number of convective timescales required to reach steady state. For the DEMON at cruise the relevant convective times for CC and FTV are 20ms and 0·2ms, respectively. Assuming five convective timescales are required to reach steady state then the relevant aerodynamic delays for CC and FTV are of the order of 100ms and 1ms respectively. The time taken for the jet to reach steady state speed following valve opening depends on the length of pipe from the valve to slot exit and the speed of sound. As the relevant valve-slot distances for CC and FTV are around 10cm this gives a time delay of around 0·3ms. Lastly, the time delay associated with fully opening or closing the control valves is around 200ms. Thus for both CC and FTV the control response dynamics is driven by the speed of response of the valve. The benefit to the overall aircraft dynamic response through increasing the CC valve response time is relatively modest; however, there are potentially significant benefits in trying to reduce the FTV valve response time.

5.0 DISCUSSION OF VEHICLE INTEGRATION AND SCALING ISSUES

5.1 Integration

This section focuses on the integration cost of implementing CC and FTV on the DEMON flight vehicle, principally in terms of the mass added to the vehicle. Subsequent analysis of performance, payload range and manoeuvrability can be undertaken once changes to the vehicle empty weight and drag are know, however these are not considered further in this paper. A significant difference between flapped and fluidic controls is that the power requirement, and hence mass cost associated with power provision, is much higher for fluidic controls. This power cost is reduced by increasing the efficiency (gain) of the fluidic controls and good progress has made in this respect in the work reported in this paper. As such, there is probably limited scope to significantly improve the highest achieved gain values of around 30 for both CC and FTV.

Unlike the aerodynamic design of the CC and FTV, the physical structures, pipe work and control valves associated with the CC

https://doi.org/10.1017/S0001924000003365 Published online by Cambridge University Press

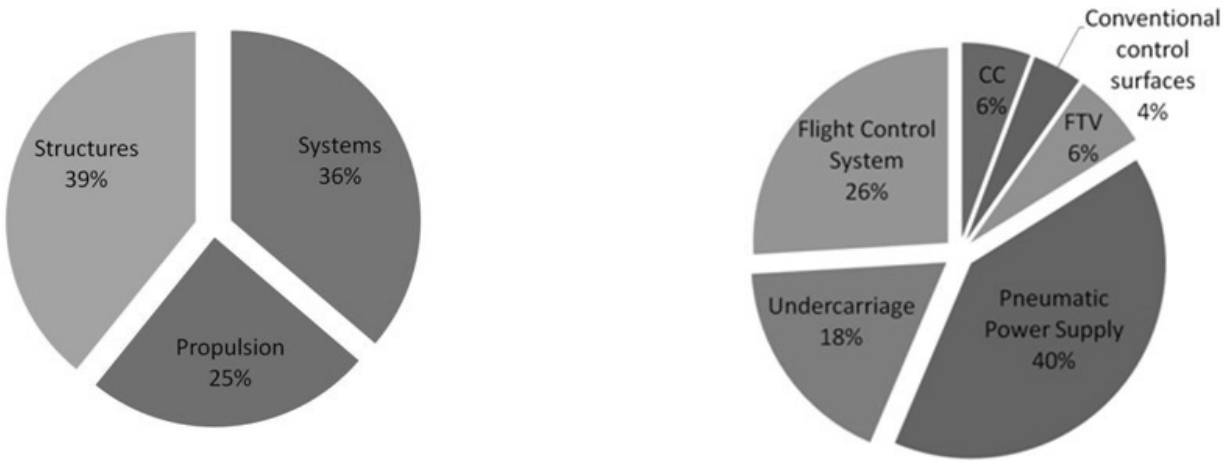

a) Overall vehicle mass breakdown. b) Vehicle systems mass breakdown.

Figure 11. Illustration of the mass contribution of vehicle systems to the DEMON overall mass, and the relative contribution of the CC and FTV systems to the systems mass.

and FTV implementation are far from optimum and there is significant room for improvement. In particular, the control valve units are based on the use of a flight control surface servo attached to a COTS ball valve designed for domestic plumbing applications. Similarly, the pipe work and connectors were limited by COTS availability and ease of installation. The CC units themselves were for convenience sized to fit in the volume of the existing flapped controls. Given the understanding of plenum design developed during this work it is clear that the chordwise extent of the plenums could be reduced significantly, perhaps down to around 25% of the current size with little decrease in internal aerodynamic performance. For the FTV nozzle, the added mass compared to a non FTV variant comes from the plenum chambers and reaction surfaces. The current reaction surface design is reasonably structurally efficient and there are probably modest opportunities for weight reduction. The plenum chambers, however, are probably significantly larger than needed and hence there are opportunities for weight reduction here.

A decision was made within the project to include a dedicated pneumatic supply system on the aircraft based around a second smaller micro gas turbine engine acting as an APU (Auxiliary Power Unit) as well as a bleed system from the main propulsive engine. The motivation for doing this was decoupling of the pneumatic supply from the engine thrust condition, such that air for the CC units could be provided for roll and pitch control during landing when the throttle was close idle and the available bleed very limited. This was a pragmatic solution for a research aircraft; however, this is unlikely to be a viable solution for a production aircraft. Aside from increasing the engine bleed performance at low throttle settings, there remains the possibility of using electrical off take from the engine to drive local air compressors where compressed air is needed. There are mechanical efficiency issues here; however, there are considerable savings in transmitting power electrically compared to pneumatically which will offset this.

To illustrate the mass cost of installing CC and FTV on to the DEMON, a basic weight breakdown analysis was conducted, Fig. . The overall aircraft mass is broken down in three main categories: Structures, Propulsion and Systems, Fig. 11(a). The Propulsion category includes the engine and jet pipe, and the fuel mass, and the Systems category includes everything else that is not structure. The Systems category is broken down into further constituents in Fig. 11b). Note that the contribution of the mass of the CC units and FTV nozzle is relatively modest (16% of systems total) compared to the mass of the dedicated Pneumatic Power Supply (40% of systems total). In terms of the overall aircraft mass, the combined mass of the dedicated CC and FTV components contribute 6%. The pneumatic power supply contributes 14% of the overall vehicle mass. This includes the FTV mass incorporating the growth in jet pipe weight due to the high AR nozzle and the reaction surfaces. All pipes/actuators are included within the PPS mass only.

5.2 Scaling

Given that the DEMON is a demonstrator aircraft rather than a practical UCAV, it is relevant to consider what additional scaling issues may need to be addressed before CC and FTV can be applied in practice. For practical UCAVs it is likely that the thrust to weight ratio will be higher (closer to 1 for a UCAV compared to around 0·3 for DEMON), and the wing loading will also be higher (e.g. around $1kNm^{-2}$ for a UCAV compared to $0{\cdot}25kNm^{-2}$ for DEMON). Increasing thrust to weight ratio implies greater installed engine power and hence this is likely to increase the margins for power off take for fluidic controls. Increased wing loading implies a greater cruise speed and hence more engine mass flow will be required to obtain a given control momentum coefficient ($C\mu$). However, given that the engine power will be sized to match the cruise (or dash) requirements then it is likely that similar levels of engine bleed will be required for similar performance requirements as determined for the DEMON aircraft. A caveat to this is that CC jet speeds are limited to low supersonic due to the problem of shock induced separation. This effectively limits the maximum free stream speed for practical CC applications to high subsonic

There is a particular issue for FTV in that higher performance aircraft will use engines with higher (supercritical) nozzle pressure ratios. This presents additional constraints on the FTV system that are beyond the scope of the present work however the basic principles established here still hold.

6.0 CONCLUSIONS

1. The flow physics associated with CC and FTV manoeuvre effectors are fundamentally similar, with both using a high aspect ratio curved wall jet to control an outer flow. For the CC system, the outer flow is the free stream flow over the wing, whereas for the FTV system the outer flow is the jet exhaust from the propulsive system. Because the flow physics are similar, it is appropriate to use a broadly similar design method for each.

https://doi.org/10.1017/S0001924000003365 Published online by Cambridge University Press

2. The integrated CC and FTV design methodology presented in this paper provides a framework for including relative control drag penalty, plenum performance metrics, and PPS system requirements as part of a design cost function. This enables trade of control efficiency against implementation cost and supports global optimisation of the overall vehicle system.
3. Prototype CC and FTV flight hardware has been successfully designed, manufactured and ground tested. Considerable engineering effort is required to implement the precise blowing slot geometry required for effective and efficient control operation. Slot geometry for both CC and FTV hardware is created by compressing the slot lip against spacers rather than by direct attachment. The CC unit also includes the provision of flexible streamwise slits in the upper and lower cover plates to reduce compressive stresses, reducing the degree of slot buckling under load.
4. For CC systems, the present work has shown that it is possible to implement effective and efficient control using a trailing edge radius sufficiently small that there is negligible increase in drag compared to the equivalent sharp trailing edge. This is a significant result in that previous CC installations on aircraft have typically used fairly large trailing edge radii that have resulted in significant drag penalties. This means that the key design driver for CC is the required mass flow rather than the installed drag penalty.
5. For FTV systems, effectiveness is driven by the termination angle of the reaction surfaces and efficiency is driven by the primary jet slot curvature. This leads to the requirement for relatively large reaction surfaces (compared to CC systems), and hence the FTV design solution may be driven by base drag cost penalty rather than mass flow requirements.
6. The CC control response is monotonic, with decreasing gradient with increasing C_μ. The peak CC gain of around 40 is achieved at low blowing rates. At higher blowing rates consistent with useful control inputs, e.g. sufficient to generate a delta C_L of around 0·1, the control gain reduces to around 10.
7. The FTV control response is 'N' shaped with a reverse control region (negative gain) in the middle and a forward control region (positive gain) either side. The peak control authority achievable in the reverse and forward control regimes is similar, however the gain obtained in the reverse region is around 30, compared to a peak gain of 3 in the forward control regime. Importantly, whilst the control gain in the reverse control regime is high, the response is sufficiently linear to allow integration of FTV into a relatively simple flight control scheme.
8. Implementation of CC and FTV as the primary manoeuvre effectors on an 80kg class gas turbine powered demonstrator aircraft has shown that added mass cost of the CC and FTV hardware is relatively modest (6% of all up weight), however the mass cost of the required pneumatic power system is more significant (15% of all up weight).
9. The pneumatic power requirements of the CC and FTV for full authority control can be met by an engine bleed system for flight conditions where throttle is significantly above idle. However, at low throttle conditions, e.g. landing, there is insufficient bleed available to service CC requirements. This has led to the inclusion of an additional APU-based PPS on the aircraft which adds significant mass penalty to the system. Implementation of fluidic controls on a production aircraft would necessitate development of an engine bleed system capable of efficient operation at low throttle settings or provision of a suitable electrical power distribution and conversion system.

ACKNOWLEDGEMENTS

This work was sponsored as part of the BAE SYSTEMS/EPSRC FLAVIIR project.

REFERENCES

1. JOSLIN, R.D. and JONES, G.S. *Applications of Circulation Control Technology*. AIAA, Progress in Astronautics and Aeronautics Series, 2006.
2. ENGLAR, R.J. Circulation control for high lift and drag generation on STOL aircraft, *J Aircr*, 1975, **12**, (5), pp 457-463.
3. ENGLAR, R.J. Development of the A-6/circulation control wing flight demonstrator configuration, TAYLOR, D.W. Naval Ship Research and Development Center, Bethesda, MD, USA, DTNSRDC/ASED-79/01, 1979.
4. ENGLAR, R.J. and HUSON, G.G. Development of advanced circulation control wing high-lift airfoils, *J Aircr*, 1984, **21**, (7), pp 476-483.
5. ENGLAR, R.J., TROBAUGH, L.A. and HEMMERLY, R.A. STOL potential of the circulation control wing for high-performance aircraft, *J Aircr*, 1978, **15**, (3), pp 175-181.
6. LOTH, J.L. Circulation control STOL aircraft design aspects, N88-17610, NASA Circulation Control Workshop, 1986.
7. LOTH, J.L., FANUCCI, J.B. and ROBERTS, S.C. Flight performance of a circulation controlled STOL aircraft, *J Aircr*, 1976, **13**, (3), pp 169-173.
8. ASBURY, S.C. and CAPONE, F.J. Multiaxis thrust-vectoring characteristics of a model representative of the F-18 high-alpha research Vehicle at angles-of-attack from 0 deg to 70 deg, NASA Langley Research Center, NASA-TP-3531, USA, 1995.
9. BARE, E.A. and REUBUSH, D.E. Static internal performance of a two-dimensional convergent-divergent nozzle with thrust vectoring, NASA Langley Research Center, NASA-TP-2721, USA, 1987
10. BERRIER, B.L. and RE, R.J. A review of thrust-vectoring schemes for fighter applications, AIAA-1978-1023, American Institute of Aeronautics and Astronautics and Society of Automotive Engineers, Joint Propulsion Conference, Las Vegas, Nevada, USA, 25-27 July, 1978.
11. BERRIER, B.L. and TAYLOR, J.G. Internal performance of two nozzles utilising Gimbal concepts for thrust vectoring, NASA Langley Research Center, NASA-TP-2991, USA, 1990.
12. RE, R.J. and LEAVITT, L.D. Static Internal Performance including thrust vectoring and reversing of two-dimensional convergent-divergent nozzles, NASA Langley Research Center, NASA-TP-2253, USA, 1984.
13. DEERE, K.A. Summary of Fluidic Thrust Vectoring Research Conducted at NASA Langley Research Center, AIAA-2003-3800, 21st AIAA Applied Aerodynamics Conference, Orlando, FL, USA, 23-26 June 2003.
14. GILL, K. The Development of Coflow Fluidic Thrust Vectoring Systems, PhD Thesis, School of Mechanical, Aerospace and Civil Engineering, The University of Manchester, Manchester, UK, 2008.
15. MASON, M.S. and CROWTHER, W.J. Fluidic thrust vectoring for low observable air vehicles, AIAA-2004-2210, 2nd AIAA Flow Control Conference, Portland, Oregon, USA, 28-1 June 2004.
16. VAN DER VEER, M.R. and STRYKOWSKI, P.J. Counterflow thrust vector control of subsonic jets: continuous and bistable regimes, *J Propulsion and Power*, 1997, **13**, (3), pp 412-420.
17. RAYMER, D.P. *Aircraft Design: A Conceptual Approach. 3rd Ed*, AIAA Education Series, Reston, VA, USA, 1999.
18. ENGLAR, R.J., HEMMERLY, R.A., MOORE, W.H., SEREDINSKY, V., VALCKENAERE, W. and JACKSON, J.A. Design of the circulation control wing STOL demonstrator aircraft, *J Aircr*, 1981, **18**, (1), pp 51-58.
19. HOERNER, S.F. *Fluid-Dynamic Drag: Theoretical, Experimental and Statistical Information*, Hoerner Fluid Dynamics, Bakersfield, CA, 1965.
20. COOK, M.V., BUONANNO, A. and ERBSLOH, S.D. A circulation control actuator for flapless flight control, *Aeronaut J*, 2008, **112**, (1134), pp 483-489.
21. FRITH, S. Flapless Control for Low Aspect Ratio Wings, PhD Thesis, School of Mechanical, Aerospace and Civil Engineering, The University of Manchester, Manchester, UK. 2007.
22. JONES, G.S. Pneumatic Flap Performance for a 2D Circulation Control Airfoil, Steady and Pulsed. 2004 NASA/ONR Circulation Control Workshop, Part 2, pp. 845-888 NASA Langley Research Center, Hampton, VA, USA, 2005.

23. WOODS, P. FLAVIIR – An integrated programme of research for UAVs, AIAA 2006-3504, 3rd AIAA Flow Control Conference, San Francisco, CA, USA, 5-8 June, 2006.
24. MICHIE, S.N. A design methodology for circulation control manoeuvre effectors, PhD Thesis, School of Mechanical, Aerospace & Civil Engineering, The University of Manchester, Manchester, UK, 2009.
25. ENGLAR, R.J. Two-dimensional subsonic wind tunnel investigations of a cambered 30% thick circulation control airfoil, Naval Ship Research and Development Center: Aviation and Surface Effects Dept, Bethesda, MD, USA, TN-AL-201, 1972.
26. ESDU. Program for the calculation of aileron rolling moment and yawing moment coefficients at subsonic speeds, Engineering Sciences Data Unit, 2006, 88040(A04), pp 1-10.
27. ESDU. Estimation of Rolling Manoeuvrability, Engineering Sciences Data Unit, 1992, EG 8/2.
28. ESDU. Stability Derivative, Lp, Rolling Moment due to Rolling for Swept and Tapered Wings, Engineering Science Data Units, A 06.01.01.
29. MILLER, D.S. *Internal Flow System,* 2nd Ed, BHR Group Limited, 1990.
30. LYTTON, A. Fluidic Thrust Vectoring of High Aspect Ratio Underexpanded Jets, PhD Thesis, School of Mechanical, Aeronautical and Civil Engineering, The University of Manchester, Manchester, UK. 2006.
31. GILL, K.G., WILDE, P.I.A. and CROWTHER, W.J. Development of an Integrated Propulsion and Pneumatic Power Supply System for Flapless UAVs AIAA-2007-7726, 7th AIAA Aviation Technology, Integration and Operations Conference (ATIO), Belfast, Northern Ireland, UK, 18-20 September 2007.
32. LOTH, J.L. and BOASSON, M. Circulation controlled STOL wing optimisation, *J Aircr*, 1984, **21**, (2), pp 128-134.
33. SPARKS, R., MICHIE, S., GILL, K., CROWTHER, W.J. and WOOD, N.J. Development of an integrated circulation control/fluidic thrust vectoring Flight Test DEMONstrator, CEIAT 2005-0086, 1st International Conference on Innovation and Integration in Aerospace Sciences, Queen's University Belfast, Northern Ireland, UK, 4-5 August 2005.
34. WILDE, P.I.A., GILL, K., MICHIE, S. and CROWTHER, W.J. Integrated design of fluidic flight controls for a gas turbine powered aircraft AIAA-2008-164 46th AIAA Aerospace Sciences Meeting and Exhibit, Reno, Nevada, USA, 7-10 January, 2008.
35. WILDE, P.I.A., GILL, K.G., MICHIE, S., SPARKS, R. and CROWTHER, W.J. Integrated design of a model-scale gas turbine powered flapless demonstrator aircraft: A Case Study AIAA-2007-7727, 7th AIAA Aviation Technology, Integration and Operations Conference (ATIO), Belfast, Ireland, UK, 18-20 September, 2007.
36. HARVELL, J.K. and FRANKE, M.E. Aerodynamic characteristics of a circulation control elliptical airfoil with two blown jets, *J Aircr*, 1985, **22**, (9), pp 737-742.
37. SOBESTER, A. and KEANE, A. Multi-objective optimal design of a fluidic thrust vectoring nozzle, AIAA-2006-6916, 11th AIAA/ISSMO Multidisciplinary Analysis and Optimisation Conference, Portsmouth, Virginia, USA, 6-8 September, 2006.
38. BURLEY, J.R. Circular to rectangular transition ducts for high aspect ratio non-axisymmetric nozzles, AIAA-1985-1346, SAE, ASME & ASEE joint propulsion conference, 1985.
39. ENGLAR, R.J. Investigation into and application of the high velocity circulation control wall jet for high lift and drag generation on STOL aircraft, USA, 1974.
40. WILDE, P.I.A., CROWTHER, W.J., BUONANNO, A. and SAVVARIS, A. Aircraft control using fluidic maneuver effectors, AIAA-2008-6406, AIAA Applied Aerodynamics Conference, Honolulu, HI, USA, 18-21 August, 2008.
41. FEARS, S.P., ROSS, H.M. and MOUL, T.M. Low-speed wind-tunnel investigation of the stability and control characteristics of a series of flying wings with sweep angles of 50°deg, NASA Langley Research Center, NASA-TM-4640, 1995.

https://doi.org/10.1017/S0001924000003365 Published online by Cambridge University Press